Data-driven numerical simulation and evaluation methods for mechanical properties of corroded high-strength steel wire for bridge cable structure

Data-driven numerical simulation and evaluation methods for mechanical properties of corroded high-strength steel wire for bridge cable structure

Zhijie Yuan, Hao Wang, Lingxiao Wang, Rou Li and Jianxiao Mao
Key laboratory of Concrete and Prestressed Concrete Structures of Ministry of Education, Southeast University, Nanjing, China, and
Stefano Invernizzi
Department of Structural, Geotechnical and Building Engineering, Politecnico di Torino, Turin, Italy

Abstract

Purpose – Cables composed of parallel steel wires are easily subject to environmental corrosion, which leads to a decrease in the bearing capacity and seriously affects the safe operation. This paper aims to propose a data-driven numerical method and evaluation framework for the mechanical properties of corroded cable structures.

Design/methodology/approach – Based on the stress-corrosion test data, a data-driven prediction method for the corrosion characteristic parameters of high-strength steel wire was proposed. According to the prediction results of corrosion morphology parameters, an ABAQUS plug-in was developed to form random corrosion pits on the surface of steel wire, and then a numerical simulation method for corroded steel wire was proposed. Combined with the monitoring data, a mechanical properties evaluation method for the corroded cable structure was constructed with corrosion time and stress level as input values.

Findings – The accuracy of the proposed method was verified by comparing the calculated results with the experiment. The gradient boosting decision tree model is the best for predicting the mechanical properties of corroded cables. The mechanical properties of steel wires decrease with increasing corrosion level. The proposed framework can accurately calculate the performance degradation of cable structures at different service stages.

Originality/value – The proposed method does not require a large number of expensive tests. Through numerical calculations combined with monitoring data, the mechanical properties of the steel wire inside the cable can be evaluated. The conclusion can provide a reference for performance assessment and maintenance decision-making of bridge structures.

Keywords High-strength steel wire, Machine learning, Random corrosion, Numerical simulation method, Mechanical properties, Monitoring and evaluation

Paper type Research paper

1. Introduction

A cable structure is usually composed of parallel steel wires, which bears the load from the girder and is the lifeline of the long-span cable-supported bridge (Hu *et al.*, 2023; Kang *et al.*, 2023; Li *et al.*, 2022; Xia *et al.*, 2022a, 2022b). Steel wire is a typical metal material (Huang *et al.*, 2024; Wang *et al.*, 2020, 2023; Xia *et al.*, 2023a, 2023b), which is extremely susceptible to corrosion damage, resulting in degradation of the mechanical properties of the cable structure, seriously affecting the service safety of the bridge (Dou *et al.*, 2024; Guo *et al.*, 2024; Li *et al.*, 2021; Yuan *et al.*, 2023). There have been many reports of structural failures of metal materials due to corrosion around the world (Li *et al.*, 2024a; Mei *et al.*, 2023; Tang *et al.*, 2024; Wu *et al.*, 2023; Yuan *et al.*, 2024a, 2024b). Therefore, it is of great engineering significance to predict the mechanical properties of corroded steel wires and evaluate the operating status of cables during service life.

Numerous bridge safety accidents and cable replacement projects have drawn people's attention to the degradation of mechanical properties of corroded cable structures and the status assessment (Ge *et al.*, 2024; Invernizzi *et al.*, 2022; Jiang *et al.*, 2020; Sun *et al.*, 2022; Yuan *et al.*, 2022). Many scholars

The current issue and full text archive of this journal is available on Emerald Insight at: **https://www.emerald.com/insight/0003-5599.htm**

Anti-Corrosion Methods and Materials

[DOI 10.1108/ACMM-12-2024-3153]

The authors gratefully acknowledge the support from the National Natural Science Foundation of China (Grant No. 52338011 and 52408159), the Natural Science Foundation of Jiangsu Province (Grant No. BK20241334), the Postgraduate Research and Practice Innovation Program of Jiangsu Province (No. SJCX23_0067) and the China Scholarship Council.

Declaration of competing interest: The authors declare that they have no known competing financial interests or personal relationships that could have appeared to influence the work reported in this paper.

Received 26 December 2024
Revised 17 April 2025
4 May 2025
Accepted 15 May 2025

have carried out tests on high-strength steel wires to study the corrosion behavior of steel wires and simulate the performance degradation of cables in different environments (Li *et al.*, 2020; Yu, 2024). Three methods are mainly used to obtain corroded steel wires. The first method is to obtain corroded steel wires in natural environments from cable replacement projects (Miao *et al.*, 2016) and study the types and distribution patterns of corrosion pits. This method can obtain corroded steel wire in service, but it is costly and takes a long research cycle. The second method is to artificially create corrosion pits (Nakamura *et al.*, 2004). This method is low-cost and easy to operate, but it ignores the randomness of corrosion behavior. The third method is to simulate the atmospheric environment and conduct salt spray corrosion tests (Xue *et al.*, 2020). Then, steel wires under different corrosion times can be obtained, and mechanical studies can be carried out. This method can simulate atmospheric environment and has relevant theoretical basis (Yuan *et al.*, 2023) to calculate the equivalent relationship between test and natural environment. At present, conducting corrosion tests is the mainstream method for studying the corrosion behavior of steel wires.

Over the past decade, a large number of corrosion tests on high-strength steel wires in stress-free state have been carried out to study the mechanical properties or fatigue mechanism of cables (Cui *et al.*, 2020; Liu *et al.*, 2021). The damage of the cable belongs to the category of stress-corrosion. When conducting artificial accelerated corrosion tests, combining different stress level conditions can more realistically simulate the corrosion behavior of the cable. However, it is difficult to incorporate different stress level conditions into the test, which requires the design of a special salt spray test chamber and its anchoring measures for the specimen. To overcome this problem, Li *et al* (2024b) fabricated a test chamber with a high-strength anchoring system and designed a stress corrosion test for high-strength steel wire. The corrosion characteristics of the specimen surface were studied, and mechanical properties tests were carried out to investigate the degradation of bearing capacity due to stress-corrosion (Li *et al.*, 2024c; Yuan *et al.*, 2025). The innovation of this study is that it considers the effect of stress level on the corrosion behavior of steel wire and proposes mechanical property indexes. At the same time, it provides a valuable database for the predictive modeling in this paper.

Although the mechanical properties of steel wires with different damage degrees can be obtained by experiments, the time and economic costs are expensive (Ma *et al.*, 2023; Yu *et al.*, 2023). To reduce the cost and quickly complete the modeling and analysis, it is necessary to develop an innovative method to predict the corrosion behavior of high-strength steel wires. As the computational paradigm with strong self-learning capabilities, machine learning (ML) methods have been widely used in the prediction of mechanical properties (Zhu *et al.*, 2024), which can help avoid repetitive and redundant experiments, aligning with the low-carbon and environmentally friendly trend. Then, numerical modeling of corroded steel wire can be studied through the mathematical indicators and the randomness of corrosion behavior. Finally, a framework for rapid evaluation of the mechanical properties of corroded cables can be proposed by combining monitoring methods with finite element (FE) analysis. However, this topic is rarely discussed due to the difficulty in simulating randomness of corrosion and the technical barriers to converting monitoring data into the test environment.

In this paper, a prediction model for the corrosion behavior of high-strength steel wire was proposed based on ML, taking the corrosion time and stress level as input characteristic values. The morphology and mechanical indicators of corroded steel wire under different environments are obtained. A numerical simulation plug-in under different mechanical indicators was developed based on Python and embedded in ABAQUS to realize the generation of random corrosion pits on the surface of steel wire. The advantages of FE method and prediction method were analyzed. Combining with monitoring data, a data-driven framework for rapid assessment of the service status of corroded cable was proposed.

2. Data-driven prediction for mechanical properties of corroded steel wire

To establish the accurate prediction model for the corrosion behavior, several specific morphological and mechanical property indicators were defined. Four ML methods are proposed, and several mathematical indicators are defined to evaluate the performance and accuracy of different prediction models.

2.1 Indicator determination

The research team conducted stress-corrosion tests on high-strength steel wires and collected the surface morphology of the corroded steel wires by 3D scanning and made some of the test data public (Li *et al.*, 2024c). This work adopted a unique experimental scheme and innovatively considered the effects of different stress levels on corrosion, providing a valuable database. Based on test results of the corroded wires, some mechanical indicators that characterize the corrosion behavior are proposed, as shown in Table 1.

Corrosion degree depends on corrosion time and stress level, which are set as input characteristic values. The parameter indicators in Table 1 are output characteristic values. A database was established for the collected test results for training and prediction. Intuitively, with the increase of corrosion time and stress level, morphological indicators such as pit depth gradually increase, while mechanical performance indicators gradually decrease.

2.2 Data-driven approach

Figure 1 illustrates the process for the data-driven approach to corrosion prediction. The collected data needs to be error-handled and normalized and then will be fed into training phase, involving random forest (RF), gradient boosting decision tree (GBDT), convolutional neural network (CNN) and support vector machine (SVM). Specific mathematical metrics are used to assess the predictive performance of each model during evaluation phase.

2.2.1 Machine learning method

2.2.1.1 Random forest. RF improves decision tree performance by combining predictions from multiple trees, as shown in Figure 2. Input data undergoes bootstrap sampling and feature selection to train individual trees, and the final output is the combination of predictions. For regression tasks, the final prediction is the average of the predictions from all decision trees, as shown in equation (1):

Table 1 Definition of corrosion behavior indicators

Morphological indicators			Mechanical indicators		
Description	**Symbol**	**Unit**	**Description**	**Symbol**	**Unit**
Quality damage rate	M	%	Elastic modulus	E	GPa
Average cross-sectional loss rate	ω_{ave}	%	Yield strength	f_y	MPa
Maximum cross-sectional loss rate	ω_{max}	%	Ultimate strength	f_u	MPa
Minimum cross-sectional loss rate	ω_{min}	%	Yield strain	ε_y	/
Average corrosion depth	h_{ave}	mm	Ultimate strain	ε_u	/
Maximum corrosion depth	h_{max}	mm	Fracture strain	ε_f	/

Source(s): Authors' own work

Figure 1 Data-driven approach

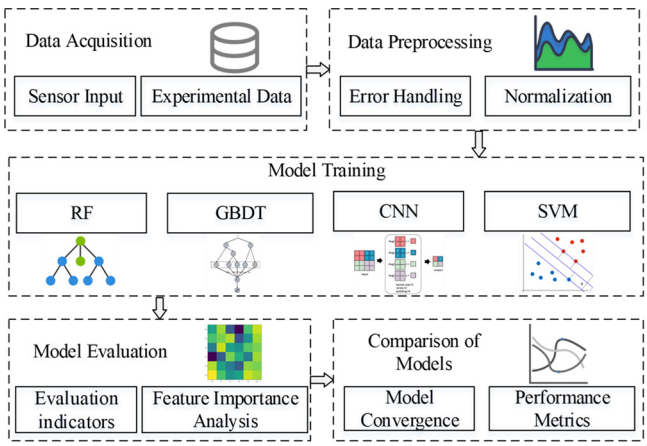

Source: Authors' own work

$$\hat{y} = \frac{1}{n}\sum_{i=1}^{n} T_i(x) \tag{1}$$

where $T_i(x)$ represents the prediction of the ith tree for input x, and n is the total number of trees. For classification tasks, the final prediction is determined by majority voting across the trees:

$$\hat{y} = \text{mode}\{T_1(x), T_2(x), \ldots, T_n(x)\} \tag{2}$$

In this study, the RF model was trained using 100 decision trees, with a maximum depth of 10 and a minimum of five samples required to split an internal node. A fixed random seed was used to ensure reproducibility. These hyperparameters were selected through grid search to optimize the model's performance and enhance its generalization ability for predicting corrosion-related indicators.

2.2.1.2 Gradient boosting decision tree. GBDT builds trees sequentially, correcting errors from previous iterations by fitting new trees to the residuals, as illustrated in Figure 3.

For regression tasks, this optimization can be mathematically expressed as equation (3):

$$F_m(x) = F_{m-1}(x) + v \cdot h_m(x) \tag{3}$$

where $F_m(x)$ is the model prediction after m iterations, $h_m(x)$ is the newly added tree and v is the learning rate that controls the contribution of each tree.

For classification tasks, GBDT uses a classification-specific loss function, such as logistic loss. The model aggregates the predictions of all trees to determine the final class. The prediction for a binary classification task can be given by equation (4):

Figure 2 Principle of RF

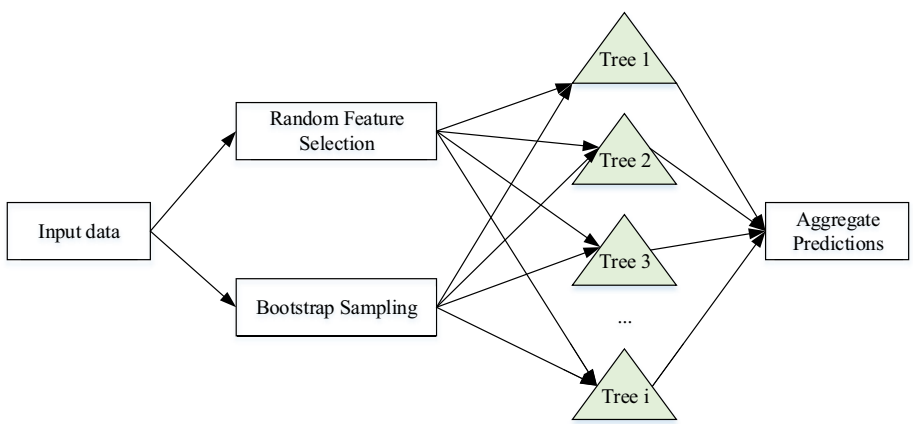

Source: Authors' own work

Figure 3 Principle of GBDT

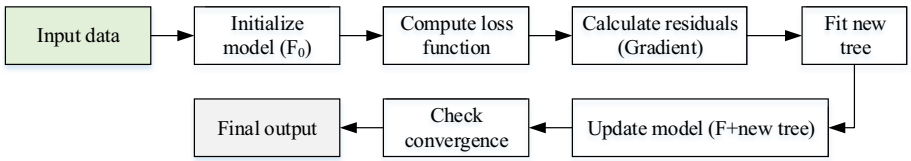

Source: Authors' own work

$$\hat{y} = sign\left(\sum_{m=1}^{M} v \cdot h_m(x)\right) \tag{4}$$

where the sign of the sum of tree outputs determines the predicted class. This approach ensures that the hardest-to-classify examples receive the most attention in each iteration.

In this study, the GBDT model was configured with 200 boosting iterations, a learning rate of 0.05, a maximum tree depth of 5, a subsampling rate of 80% and a minimum of ten samples per leaf node. These parameters were fine-tuned using cross-validation to ensure an effective trade-off between prediction accuracy and model complexity in the corrosion prediction tasks.

2.2.1.3 Convolutional neural networks. A CNN was used to capture the spatial correlation and hierarchical features within the input data. The architecture consists of multiple layers, including convolutional layers, activation functions, pooling layers, a flattening step and fully connected layers (Figure 4). The convolutional layers act as feature extractors that preserve the local dependencies of the input while reducing dimensionality through pooling operations. This hierarchical design enables the model to learn increasingly abstract representations of the data.

The forward propagation process in the convolutional layer can be mathematically expressed as:

$$Z^{(l)} = f\left(W^{(l)} * X^{(l-1)} + b^{(l)}\right) \tag{5}$$

where $Z^{(l)}$ denotes the output of layer l, $W^{(l)}$ and $b^{(l)}$ are the weights and biases, $*$ represents the convolution operation and $f()$ is the nonlinear activation function (e.g. ReLU). After the feature extraction process, the data is flattened and passed to fully connected layers to perform final regression prediction. The network was trained using a backpropagation algorithm to minimize the loss function, ensuring effective feature learning and stable performance.

In this study, the CNN model consisted of two convolutional layers, each containing 32 filters of size 3 by 3, followed by max-pooling layers with a 2 by 2 window. The activation function used was ReLU, and a fully connected layer with 64 units was followed by a linear output layer for regression tasks. The model was trained using the Adam optimizer with a learning rate of 0.001, a batch size of 32 and 100 training epochs. This configuration facilitated stable convergence and effective feature extraction from the input data.

2.2.1.4 Support vector machine. SVM is a supervised learning algorithm for classification and regression tasks, particularly effective in high-dimensional spaces. As illustrated in Figure 5, SVM identifies the optimal hyperplane that separates data points of different classes while maximizing the margin between the support vectors of each class.

For linearly separable data, this decision boundary is a straight line in 2D or a hyperplane in higher dimensions. The optimization problem for finding this hyperplane is formulated as equation (6):

$$\min_{w,b} \frac{1}{2}\|w\|^2 \tag{6}$$

Subject to the constraint:

$$y_i(w \cdot x_i + b) \geq 1, \ \forall i \tag{7}$$

where w is the weight vector, b is the bias, x_I represents the training examples and y_i are the corresponding labels. The goal is to maximize the margin between the support vectors and the hyperplane, ensuring the best possible separation between classes.

For cases where the data is not linearly separable, SVM introduces the kernel trick, which allows it to map the data into a higher-dimensional space where it can become linearly separable. The decision function in the higher-dimensional space can be expressed as equation (8):

Figure 4 Principle of CNN

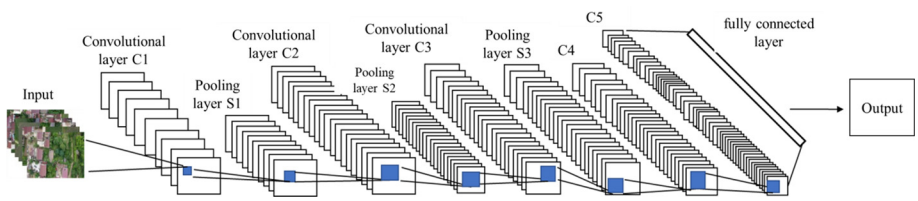

Source: Authors' own work

Figure 5 Principle of support vector machine

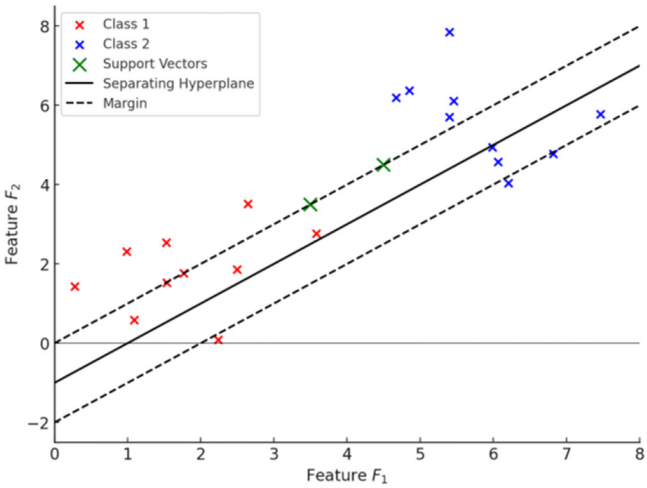

Source: Authors' own work

$$f(x) = sign\left(\sum_{i=1}^{N} \alpha_i y_i K(x_i, x) + b\right) \tag{8}$$

where $K(x_i,x)$ is the kernel function, and α_i are the Lagrange multipliers.

In this study, the SVM model adopted a radial basis function kernel, with the regularization parameter set to 10, and the kernel coefficient automatically scaled to the input data distribution. The epsilon-support vector regression setting was used to allow for a specified tolerance margin in the prediction results. These hyperparameters were determined through experimental tuning to ensure robust and stable performance in modeling the relationship between corrosion conditions and mechanical properties.

2.2.2 Data set configuration

The data set captures numerical parameters listed in Table 1. It should be noted that due to the difficulty and cost of implementing stress-corrosion tests, the original data set had a limited number of samples and exhibited irregular spacing across the input variables, which could compromise the robustness of model training. To address this issue, an interpolation-based data augmentation strategy can be adopted to enhance the generalization ability and prediction stability of ML models. The interval of corrosion days was set to 1, and the interval of stress level was set to 100. The final data set used in this study contains 1,910 samples. Additional data points are generated by interpolation methods to encrypt the feature space and improve the continuity of data distribution. In particular, the mathematical model given by Li *et al.* (2024b) can be used as the theoretical algorithm for interpolation, which has specific physical meaning and mathematical logic, and can ensure the rationality of all data samples. It is important to emphasize that interpolation-based augmentation methods have been widely used in small-shot regression tasks (Song *et al.*, 2023; Zhang *et al.*, 2022) to improve learning stability and mitigate overfitting, especially when experimental or real-world data collection is significantly limited. This approach enables each model to better capture the underlying relationship between features and the target variable, thereby improving performance on unseen data.

Figure 6 visualizes the Pearson correlation coefficients among variables related to corrosion and mechanical properties, offering a comprehensive depiction of their linear relationships and corresponding strengths. The heatmap uses a color gradient, where positive correlations are shown in red, and negative correlations in blue, with the intensity of the color indicating the magnitude of the correlation. This enables the identification of both strong and weak relationships across the data set.

The correlations depicted in the heatmap are quantified using the Pearson correlation coefficient, defined as follows:

$$r = \frac{\sum_{i=1}^{n}(x_i - \overline{x})(y_i - \overline{y})}{\sqrt{\sum_{i=1}^{n}(x_i - \overline{x})^2}\sqrt{\sum_{i=1}^{n}(y_i - \overline{y})^2}} \tag{9}$$

where x_i and y_i represent the individual values of variables x and y, $\overline{x}$ and $\overline{y}$ are respective means and n is the total number of data points.

Notably, the heatmap reveals strong positive correlations (coefficients close to 1) among corrosion-related parameters, such as "Mass Loss Rate," "Volume Loss Rate" and "Max Section Loss Rate," reflecting their consistent representation of corrosion severity. By contrast, variables representing mechanical properties, such as "Yield Strength" and "Ultimate Strength," display pronounced negative correlations (coefficients close to −1) with key corrosion parameters like "Max Corrosion Depth" and "Avg Corrosion Depth." This underscores the detrimental impact of increasing corrosion severity on material performance. Moreover, the moderate positive correlations (coefficients around 0.5–0.6) between "Stress Level" and corrosion depth parameters suggest that stress can accelerate the corrosion process.

Hyperparameter settings were determined based on the combination of empirical knowledge and experimental results, aiming to optimize the predictive performance of each algorithm. Through grid search and cross-validation, these parameters were carefully adjusted to ensure robustness and accuracy in predicting the corrosion-related outputs.

2.2.3 Evaluation indicators

To comprehensively evaluate the performance of the ML models, a suite of evaluation metrics was used for both point and interval predictions, which collectively provide a nuanced assessment of the accuracy, reliability and robustness, ensuring the applicability to complex prediction tasks. For point predictions, indicators include the coefficient of determination (R^2), mean absolute error (MAE) and root mean square error (RMSE). Additionally, the mean absolute percentage error (MAPE) was used to offer a scale-independent perspective on relative prediction accuracy, complemented by the mean (MEAN), which captures the central tendency of predicted values, revealing potential biases. The coefficient of variation (COV) further assessed the stability and consistency of the predictions by examining the relative variability in predicted outputs. The following equations are used to calculate these metrics:

Figure 6 Pearson correlation coefficients for parameters

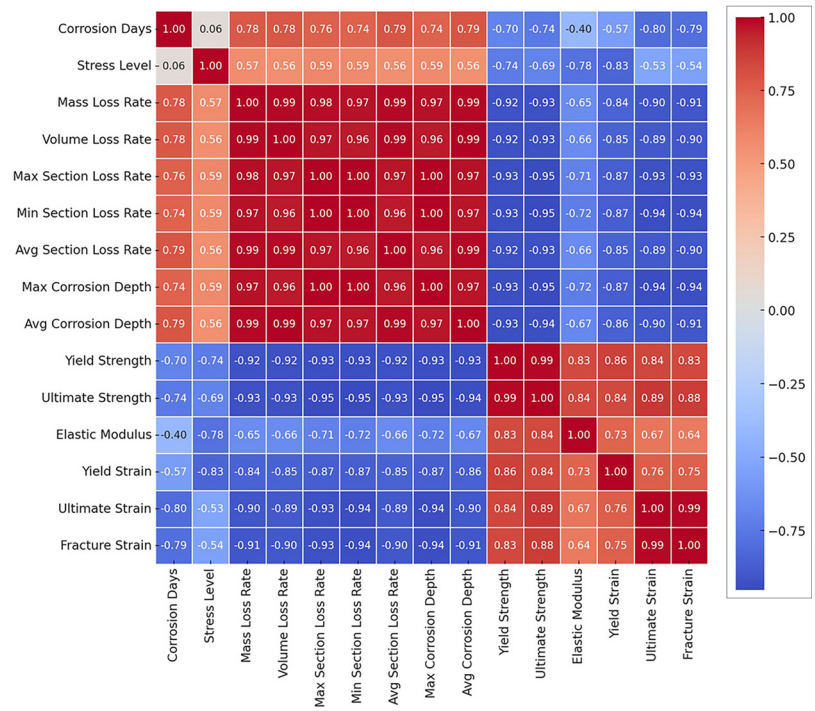

Source: Authors' own work

$$R=\frac{\sum_{i=1}^{n}\left(y_i^*-\overline{y_i^*}\right)\left(y_i-\overline{y}\right)}{\sqrt{\sum_{i=1}^{n}\left(y_i^*-\overline{y_i^*}\right)^2}\sqrt{\sum_{i=1}^{n}\left(y_i-\overline{y}\right)^2}} \tag{10}$$

$$MAE=\frac{1}{n}\sum_{i=1}^{n}\left|y_i^*-y_i\right| \tag{11}$$

$$RMSE=\sqrt{\frac{1}{n}\sum_{i=1}^{n}\left(y_i-y_i^*\right)^2} \tag{12}$$

$$MAPE=\frac{1}{n}\sum_{i=1}^{n}\frac{\left|y_i-y_i^*\right|}{y_i}\times 100\% \tag{13}$$

$$MEAN=\frac{1}{n}\sum_{i=1}^{n}y_i \tag{14}$$

$$COV=\frac{1}{n}\sum_{i=1}^{n}\left(y_i-\overline{y}\right)\left(y_i^*-\overline{y_i^*}\right) \tag{15}$$

where n represents the number of data points; y_i and y_i^* are the observed and predicted values, respectively; and $\overline{y}$ $\overline{y_i^*}$ represent the means of the observed and predicted values, respectively.

For interval predictions, two specialized metrics were adopted to evaluate the reliability and precision of the prediction intervals. The prediction interval coverage probability (PICP) measures the proportion of observed values falling within the predicted intervals, with higher PICP values reflecting robust interval reliability. Meanwhile, the normalized mean prediction interval width (NMPIW) provides a measure of the interval width normalized by the range of predictions, where lower values denote more precise intervals. PICP and NMPIW can be expressed as follows:

$$PICP=\frac{1}{n}\sum_{i=1}^{n}c_i \tag{16}$$

$$NMPIW=\frac{1}{nR}\sum_{i=1}^{n}\left[U(x_i)-L(x_i)\right] \tag{17}$$

where c_i is equal to 1 when the test value for sample i falls into the predicted interval; otherwise, it is equal to 0; $U(x_i)$ and $L(x_i)$ are the upper and lower interval boundaries for sample i, respectively; R is the variation in range of test value for gross sample.

2.3 Comparison of prediction models

As for the data set splitting, the training set, comprising 80% of the data, was used to train the models, while the remaining 20% was held out for testing to evaluate the predictive performance on unseen data. Figure 7 provides the performance of RF, GBDT, CNN and SVM in various prediction metrics. GBDT demonstrates the highest R^2 value of 0.9991, indicating the best fit to the data. It also has the lowest MAE (0.2301) and RMSE

(0.3113), suggesting that GBDT produces more accurate predictions compared to the other models. In terms of the MAPE, GBDT again outperforms the others with a value of 0.6114, while SVM has the highest error rate at 7.0992, showing less accuracy in percentage-based errors. For the mean prediction value (MEAN), all models perform similarly, but GBDT and CNN show slightly lower mean values than SVM.

In terms of interval prediction metrics, GBDT also performs the best, with a PICP of 0.93 (the highest among the models), meaning it has the highest proportion of actual values falling within the prediction intervals. Furthermore, GBDT has the narrowest prediction interval, as indicated by the lowest NMPIW of 0.12, reflecting better precision in its interval estimates. In summary, based on the combined analysis of both point and interval prediction metrics, GBDT is the most suitable model for this data set, offering the best balance of accuracy, stability and precision.

3. Numerical simulation method for corroded steel wire

3.1 Establishment of database for corrosion indicators

According to the corrosion index prediction method in Section 2, taking corrosion time and pre-strain as input features, the GBDT model was used to establish a prediction database for corrosion performance indicators of high-strength steel wires under different corrosion degrees. According to equivalent calculation (Yuan *et al.*, 2023), the corrosion time is divided into 101 levels from 0 to 100 days, with an interval of 1. The stress level is divided into 21 levels from 0 to 2,000$\mu\varepsilon$ with an interval of 100. The trained GBDT model was used to calculate the index parameters under different corrosion levels, with a total of 2,121 cases, thus forming a complete corrosion index database. An ABAQUS plug-in was developed based on Python to generate a series of random corrosion pits on the surface of high-strength steel wire. Starting from the morphological parameters listed in Table 1, the Python script calculates a statistically representative population of surface corrosion pit

Figure 7 Model evaluation metrics for RF, GBDT, CNN and SVM

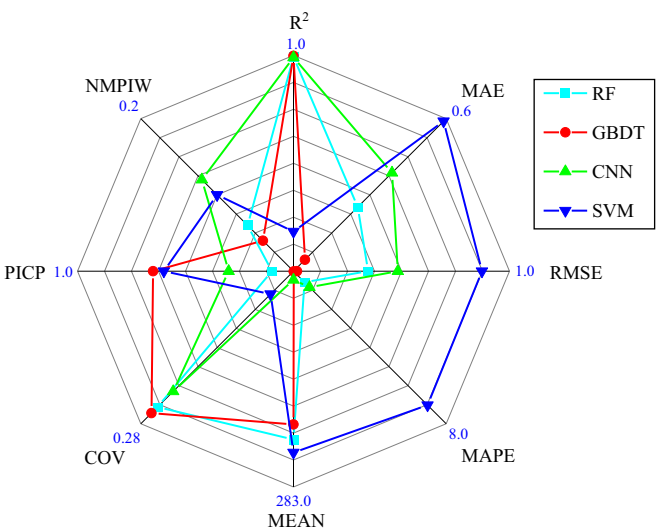

Source: Authors' own work

holes of spherical shape. These geometries are subtracted from the initial cylindrical geometry of the uncorroded sample. Finally, the mesh of a corroded sample can be obtained, which represents in a realistic way the true geometry of the corroded sample. The database establishment and modeling process is shown in Figure 8. In addition, to verify the accuracy, a method of establishing a corroded steel wire model based on the equivalent cross-section reduction is proposed. Numerical simulations were performed on different FE models, and yield strength and ultimate strength were calculated and compared with the test and prediction results.

3.2 Finite element model of corroded steel wire

The FE model of the high-strength steel wire with a diameter of 5.0 mm and a test section length of 400 mm can be established based on ABAQUS. The element type adopted hexahedral element C3D8R, and the grid size was selected as 0.1 mm (Li *et al.*, 2024a). Then, the FE model containing random corrosion pits under four corrosion levels was established by ABAQUS by embedding the Python plug-in, as shown in Figure 9. The basis for the selection is the existence of detailed experimental data that can be used to verify the correctness of the numerical analysis. Mass loss rate (M) is used to describe the degree of corrosion. The corrosion pits are evenly distributed in the test section. When building the Python script, ABAQUS modules and related libraries should be imported in advance, including os, numpy, math, matplotlib, etc. Two arrays for storing the cylindrical coordinates and Cartesian coordinates of random corrosion pits are established to obtain the corrosion pit position parameters in each cycle. The modeling can be completed until all corrosion parameters meet the database standards in Figure 8.

The material properties of the FE model are determined by the mechanical parameters and constitutive relations of the uncorroded steel wire (Li *et al.*, 2024b; Yao *et al.*, 2016). The fracture criterion adopted the flexible damage criterion. True stress and true strain can be transformed by:

$$\sigma_T = \sigma_{nom}(1 + \varepsilon_{nom}) \tag{18}$$

$$\varepsilon_T = ln(1 + \varepsilon_{nom}) \tag{19}$$

where σ_T and ε_T are the true stress and true strain, respectively; σ_{nom} and ε_{nom} are the nominal stress and strain, respectively.

In addition, another FE model of corroded steel wire based on the equivalent cross-section reduction method is also proposed. This method does not take into account the randomness of corrosion and assumes that the surface of the steel wire is smooth and uniformly corroded. The cross-sectional equivalent diameter of the corroded steel wire can be calculated as follows:

$$D = \sqrt{1 - M}D_0 \tag{20}$$

where D is equivalent diameter of the steel wire; D_0 is original diameter; M is the quality damage rate.

3.3 Comparison and validation

Figure 10 shows the comparison between the experimental results and the calculation results under different methods of the

Figure 8 Database establishment and modeling process

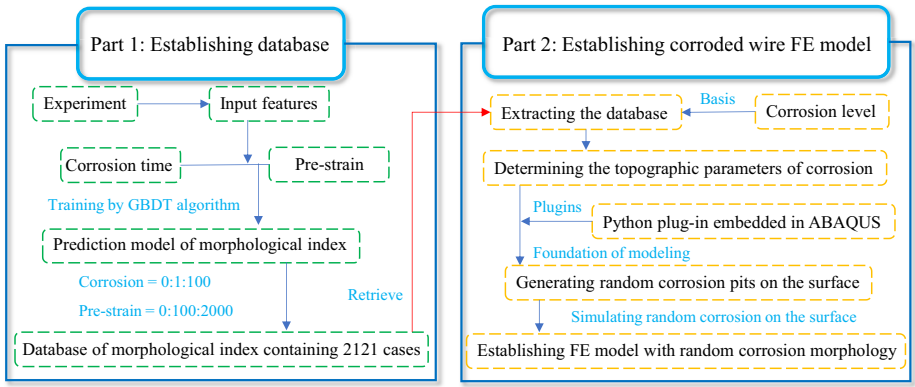

Source: Authors' own work

Figure 9 FE model of steel wire with random corrosion pits

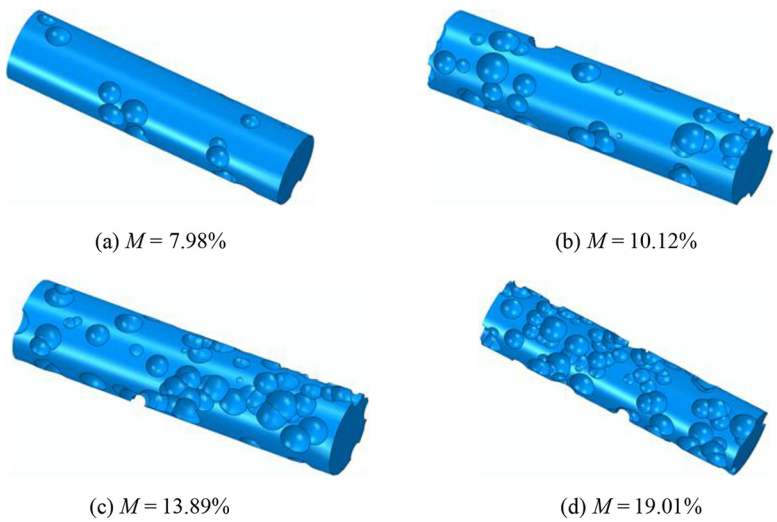

(a) $M = 7.98\%$ (b) $M = 10.12\%$

(c) $M = 13.89\%$ (d) $M = 19.01\%$

Source: Authors' own work

mechanical properties for the corroded steel wire, which includes the calculation results of the data-driven method based on GBDT and the two FE simulation methods. FE-1 means that the model is established by setting random corrosion pits, and FE-2 means that the model is established by the equivalent cross-section reduction method. In general, all three calculation methods have good accuracy. As there are no corrosion pits, the effect of stress concentration phenomenon is disregarded. Consequently, the calculation results of FE-2 may overestimate the wire strength, resulting in unsafety. Taking the corrosion degree of 7.98% as an example, for yield strength, the error between FE-1 and the test is 0.57%, while the error between FE-2 and the test is 2.46%. Therefore, when calculating the mechanical properties of corroded steel wire, the model with random corrosion pits has an advantage in accuracy.

The GBDT prediction and FE-1 method are essentially data-driven methods developed based on experimental data, so the calculation results both provide a good estimate of the wire strength. Therefore, the GBDT prediction or FE-1 method is the best option to evaluate the mechanical properties of corroded steel wire. The reason is that the prediction method based on GBDT and the FE-1 method are both essentially data-driven and take into account the corrosion days and pre-stress level. The FE-2 method only considers the mass loss rate but fails to consider the effects of corrosion days and pre-stress level. Relatively speaking, the data-driven prediction results based on GBDT are slightly better than the calculation results of FE-1. The calculation results of FE-1 are conservative because the random corrosion pits may lead to stress concentration, causing the component to yield or fracture prematurely.

4. Evaluation framework for cable service performance

The purpose of this study is to provide an evaluation framework for the mechanical properties of long-span bridge cables. The

Figure 10 Comparison of mechanical properties for corroded steel wire

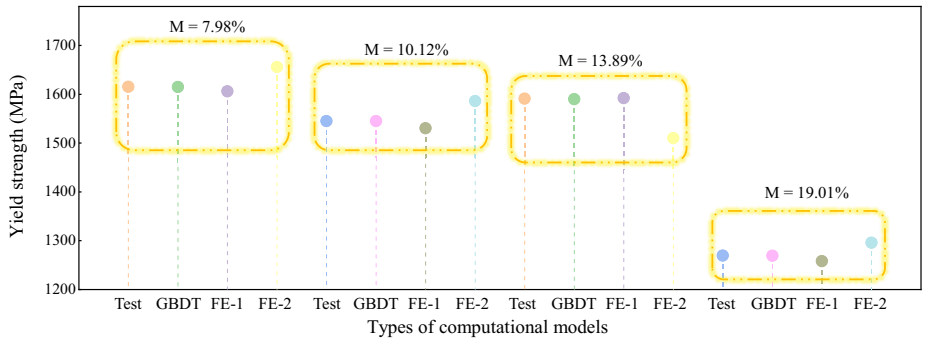

(a) Yield strength of corroded steel wire

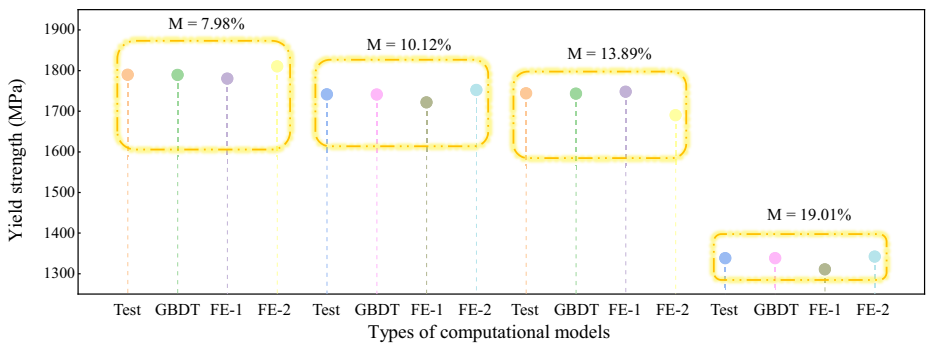

(b) Ultimate strength of corroded steel wire

Source: Authors' own work

objective is to assess the structural condition of the bridge without the need for extensive mechanical tests. According to the above, a database of corrosion morphology parameters of steel wires at different corrosion levels has been obtained, and prediction and FE analysis methods have been given. Therefore, obtaining the corrosion degree of the steel wires inside the cable structure in the actual service environment is the key to establishing an evaluation framework. The indicators for evaluating the degree of corrosion are corrosion time and stress level. In this section, the calculation method of the corrosion degree will be discussed in detail, and a detailed cable service performance evaluation process will be given.

4.1 Corrosion time

The corrosion amount of metal during electrochemical corrosion in the t1–t2 time period can be expressed as the form of integration based on Faraday's law:

$$Q = \frac{1}{F}\int_{t_1}^{t_2} I_c \, dt \tag{21}$$

where Q is the corrosion amount of metal; I_c is the corrosion current; and F is Faraday constant. It can be seen that the amount of corrosion is related to time and current intensity.

The amount of metal corrosion in the test is equal to the amount of corrosion in the actual service environment. The equivalent relationship can be derived:

$$I_{ce} \cdot t = I_{ci} \cdot T_i \tag{22}$$

where t and T_i are corrosion time in test and service environment, respectively; I_{ce} and I_{ci} are the corrosion current under the test conditions and operating environment, respectively. Then:

$$t = \frac{I_{ci}}{I_{ce}} \cdot T_i = \alpha \cdot T_i \tag{23}$$

where $\alpha = \frac{I_{ci}}{I_{ce}}$ is defined as the equivalent conversion coefficient, which is the function of temperature, RH, pH value and NaCl mass. As long as α is determined, the equivalent corrosion time can be calculated.

By combining the monitoring data to compile the environmental spectrum, the equivalent conversion coefficient and corrosion time can be calculated (Yuan *et al.*, 2023). The total corrosion time t_e under test of cable steel wire can be expressed as follows:

$$t_e = \sum_{i=1}^{n} \alpha_i \cdot t_i \tag{24}$$

where n is the combination number of different working condition values of the bridge in the operating environment according to the monitoring data. α_i and t_i are the equivalent conversion factors

and service time under different conditions, respectively. In other words, the equivalent corrosion time can be calculated by simply obtaining the corresponding monitoring data.

4.2 Stress level

The stress level of the steel wire can be obtained by calculating the cable tension. The most direct method is to collect monitoring data from cable tension sensors arranged on the cables. But the prerequisite is that sensors are installed on each cable in the health monitoring system. It can also be obtained by sampling the vibration frequency of each cable through on-site measurement (Fu *et al.*, 2017). The principle of measuring cable force by frequency method can be explained by following:

$$\omega^2 = K_1 \frac{T}{ml^2} + K_2 \frac{EI}{ml^4} \tag{25}$$

where ω is the frequency of structure; T is the cable force; K_1 and K_2 are independent constant parameters to be identified. First, the vibration curve of the cable is approximately obtained. Then, according to the basic principle that the maximum potential energy and the maximum kinetic energy of the cable during vibration are equal, the values of K_1 and K_2 can be specifically calculated by substituting the vibration curve into the energy equation.

In addition, the FE method can be used to directly calculate the cable force of each cable. The prerequisite is to establish a correct FE model. The verification method is to compare the simulation data with the monitoring data, including the static indicators and dynamic response of the structure.

4.3 Evaluation framework

So far, a complete data-driven numerical analysis method and evaluation framework for the mechanical properties of corroded high-strength steel wire have been established. The framework includes data-driven prediction methods, numerical modeling techniques and mechanical property evaluation. The static performance evaluation of the cable structure can be completed by simply obtaining relevant data from the health monitoring system, as shown in Figure 11.

The evaluation work according to this framework process does not require a large number of salt spray corrosion and mechanical tensile tests, nor does it require the dismantling and inspection of the cable structure. The mechanical properties evaluation can be completed by only obtaining monitoring data related to corrosion time and stress level factors from the structural health monitoring system.

5. Conclusion

- The GBDT model showed good prediction ability for the corrosion behavior indicators of high-strength steel wire under different corrosion times and stress levels. For the evaluation of the mechanical properties of corroded steel wire, data-driven methods are more efficient than numerical simulation methods.
- An ABAQUS plug-in for generating random corrosion pits on the surface of components was developed based on Python. A numerical simulation method for corroded steel wire was proposed. The calculation results of random corrosion pit modeling method are closer to the actual situation than the equivalent cross-section reduction

Figure 11 Framework for evaluating the mechanical properties of corroded cable

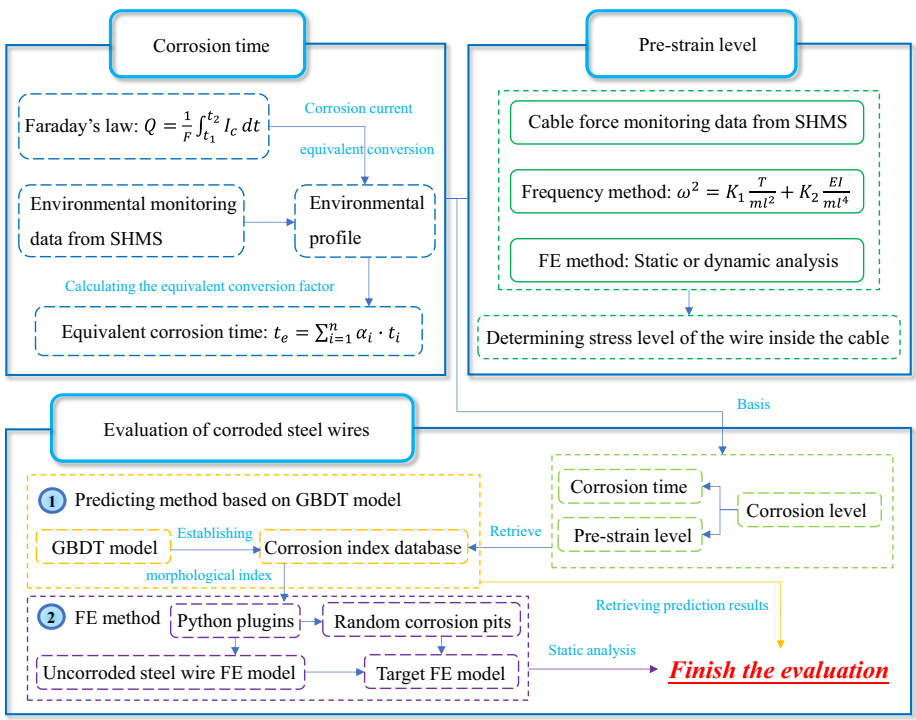

Source: Authors' own work

method. The test data, prediction results and FE calculation values are in good agreement, which proves the correctness of the method proposed in this paper. Although both have high accuracy, the numerical simulation method is more time-consuming than the GBDT prediction method.

- Based on the corrosion time and stress level, the evaluation framework for the mechanical properties of corroded steel wire was proposed. This method does not require a large number of expensive tests and bridge demolition inspections, and the assessment can be completed based solely on monitoring data.

It is worth noting that the proposed evaluation framework still has some limitations. Extreme corrosion, such as pitting penetration and stress corrosion cracking, may lead to sudden failure of material properties, and the proposed equivalent calculation method for corrosion effects may not be applicable. The proposed framework fails to consider complex stress states such as the bending-torsion coupling effect caused by wind loads. The proposed framework fails to consider uncertainties in monitoring data, such as outliers and missing data. Eliminating these limitations based on advanced theoretical algorithms and rich monitoring data will be the future research project.

References

Cui, C., Xu, Y., Zhang, Q. and Wang, F. (2020), "Vehicle-induced fatigue damage prognosis of orthotropic steel decks of cable-stayed bridges", *Engineering Structures*, Vol. 212, p. 110509.

Dou, X., Li, Y., Zhang, X., Wang, S., Cheng, Y., Yao, W., Zhang, D. and Li, Y. (2024), "The corrosion analysis of X80 pipeline steel welded joint using wire beam electrode and numerical simulation methods", *Anti-Corrosion Methods and Materials*, Vol. 71 No. 6, pp. 733-744.

Fu, Z., Ji, B., Wang, Q. and Wang, Y. (2017), "Cable force calculation using vibration frequency methods based on cable geometric parameters", *Journal of Performance of Constructed Facilities*, Vol. 31 No. 4, p. 4017021.

Ge, B., Ma, R., Zhu, Q., Chen, A. and Chang, H. (2024), "Fatigue life prediction of corroded hangers with parallel steel wire in a network arch bridge under vehicle-bridge interaction based on a novel noniterative simplified method", *International Journal of Fatigue*, Vol. 187, p. 108457.

Guo, X., Tu, J., Fan, Z., Du, B., Shang, H., An, J. and Jia, D. (2024), "Experimental and simulation analysis of mechanical property degradation of corrosion thinning of Q355 steel for transmission towers", *Anti-Corrosion Methods and Materials*, Vol. 71 No. 6, pp. 620-631.

Hu, D., Song, S., Zhang, Z. and Wang, L. (2023), "Experimental study on corrosion resistance of Zn-Al-Mg alloy coating of high-strength steel wires for bridge cables", *Anti-Corrosion Methods and Materials*, Vol. 70 No. 6, pp. 459-468.

Huang, C., Wang, Z., Yao, Z., Ma, Y., Guo, F. and Chai, L. (2024), "Facile fabrication of an enhanced electrodeposited nickel electrode for alkaline hydrogen evolution reaction", *Electrochimica Acta*, Vol. 477, p. 143792.

Invernizzi, S., Montagnoli, F. and Carpinteri, A. (2022), "Very high cycle corrosion fatigue study of the collapsed polcevera bridge, Italy", *Journal of Bridge Engineering*, Vol. 27 No. 1, p. 4021102.

Jiang, C., Wu, C., Cai, C. and Xiong, W. (2020), "Fatigue analysis of stay cables on the long-span bridges under combined action of traffic and wind", *Engineering Structures*, Vol. 207, p. 110212.

Kang, Z., Zhang, Z., Song, S., Cheng, Q., Tao, S. and Ni, Y. (2023), "Effect of pitting corrosion on the mechanical properties and fracture model of steel wires for bridge cable", *Anti-Corrosion Methods and Materials*, Vol. 70 No. 4, pp. 173-181.

Li, R., Miao, C. and Yu, J. (2020), "Effect of characteristic parameters of pitting on strength and stress concentration factor of cable steel wire", *Construction and Building Materials*, Vol. 240, p. 117915.

Li, R., Miao, C. and Wei, T. (2021), "Effect of environmental factors on electrochemical corrosion of galvanized steel wires for bridge cables", *Anti-Corrosion Methods and Materials*, Vol. 69 No. 1, pp. 111-118.

Li, R., Miao, C., Nie, M. and Wang, Y. (2022), "Equivalent relationship of accelerated corrosion and compilation method of environmental spectrum of corroded steel wires", *Anti-Corrosion Methods and Materials*, Vol. 69 No. 4, pp. 387-394.

Li, R., Wang, H., Miao, C., Yuan, Z. and Ni, Y. (2024a), "Evaluating stress corrosion damage of steel wires as bridge cables based on the corrosion surface", *Journal of Materials in Civil Engineering*, Vol. 36 No. 6, p. 4024113.

Li, R., Wang, H., Miao, C., Ni, Y. and Zhang, Z. (2024b), "Experimental and numerical study on the degradation law of mechanical properties of stress-corrosion steel wire for bridge cables", *Journal of Constructional Steel Research*, Vol. 212, p. 108294.

Li, R., Wang, H., Miao, C., Yuan, Z. and Zhang, Z. (2024c), "Three-dimensional fatigue crack initiation and propagation behavior of stress-corroded steel wires for bridge cables", *International Journal of Fatigue*, Vol. 192, p. 108717.

Liu, X., Zhang, W., Gu, X. and Ye, Z. (2021), "Probability distribution model of stress impact factor for corrosion pits of high-strength prestressing wires", *Engineering Structures*, Vol. 230, p. 111686.

Ma, Y., He, Y., Wang, G., Wang, L., Zhang, J. and Lee, D. (2023), "Corrosion fatigue crack growth prediction of bridge suspender wires using Bayesian Gaussian process", *International Journal of Fatigue*, Vol. 168, p. 107377.

Mei, X., Yan, Y. and Qiao, L. (2023), "Research on hydrogen embrittlement behavior of L-PBF 18Ni (300) maraging steel by experiments and numerical simulations", *Acta Materialia*, Vol. 256, p. 119141.

Miao, C., Yu, J. and Mei, M. (2016), "Distribution law of corrosion pits on steel suspension wires for a tied arch bridge", *Anti-Corrosion Methods and Materials*, Vol. 63 No. 3, pp. 166-170.

Nakamura, S., Suzumura, K. and Tarui, T. (2004), "Mechanical properties and remaining strength of corroded bridge wires[J]", *Structural Engineering International*, Vol. 14 No. 1, pp. 50-54, doi:10.2749/101686604777964305.

Song, X., He, Y., Li, X., Zhu, Q. and Xu, Y. (2023), "Novel virtual sample generation method based on data augmentation and weighted interpolation for soft sensing with small data", *Expert Systems with Applications*, Vol. 225, p. 120085.

Sun, G., Yuan, Z., Wu, B. and Zhao, F. (2022), "Methodology and application of safety evaluation of reinforced concrete girder bridges during earthquakes", *Shock and Vibration*, Vol. 2022 No. 1, p. 5591334.

Tang, X., Zhou, J., Jian, G., Deng, Q., Zhao, W., Mo, S., She, Z., Zhong, Y., Huang, L., Shu, C., Pan, M. and Wang, Z. (2024), "Nondestructive differential eddy current testing for corrosion detection on coated aluminium alloys", *Anti-Corrosion Methods and Materials*, Vol. 71 No. 6, pp. 855-867.

Wang, Z., Yan, Y. and Qiao, L. (2020), "Effect of deformed subsurface on the corrosion resistance of biomedical CoCrMo alloy in simulated physiological solution", *Journal of Materials Science*, Vol. 55 No. 27, pp. 13351-13362.

Wang, Z., Yan, Y., Wu, Y., Zhang, Y., Zhao, X., Su, Y. and Qiao, L. (2023), "Recent research progress on the passivation and selective oxidation for the 3d-transition-metal and refractory multi-principal element alloys", *Npj Materials Degradation*, Vol. 7 No. 1, p. 86.

Wu, Y., Wang, Z., Chen, J., Ma, Y., Yan, Y. and Qiao, L. (2023), "Effect of frictional frequency on the subsurface evolution of 316L stainless steel in tribocorrosion and its influence on the synergistic effect between corrosion and wear", *Tribology International*, Vol. 178, p. 108026.

Xia, D., Deng, C., Macdonald, D., Jamali, S., Mills, D., Luo, J., Strebl, M., Amiri, M., Jin, W., Song, Z. and Hu, W. (2022a), "Electrochemical measurements used for assessment of corrosion and protection of metallic materials in the field: a critical review", *Journal of Materials Science & Technology*, Vol. 112, pp. 151-183.

Xia, D., Deng, C., Chen, Z., Li, T. and Hu, W. (2022b), "Modeling localized corrosion propagation of metallic materials by peridynamics: progresses and challenges", *Acta Metallurgica Sinica*, Vol. 58 No. 9, pp. 1093-1107.

Xia, D., Mao, Y., Deng, C., Zhu, Y. and Hu, W. (2023a), "Localized corrosion mechanism of 2024 aluminum alloy in a simulated dynamic seawater/air interface", *Acta Metallurgica Sinica*, Vol. 59 No. 2, pp. 297-308.

Xia, D., Ji, Y., Zhang, R., Mao, Y., Behnamian, Y., Hu, W. and Birbilis, N. (2023b), "On the localized corrosion of AA5083 in a simulated dynamic seawater/air interface-part 1: corrosion initiation mechanism", *Corrosion Science*, Vol. 213, p. 110985.

Xue, S., Shen, R., Chen, W. and Miao, R. (2020), "Corrosion fatigue failure analysis and service life prediction of high strength steel wire", *Engineering Failure Analysis*, Vol. 110, p. 104440.

Yao, D., Cai, L. and Bao, C. (2016), "A new approach on necking constitutive relationships of ductile materials at elevated temperatures", *Chinese Journal of Aeronautics*, Vol. 29 No. 6, pp. 1626-1634.

Yu, X. (2024), "Study on the durability of steel wire under the coupling effects of harsh environment and variable loads", *Engineering Failure Analysis*, Vol. 157, p. 107487.

Yu, S., Yan, C., Liu, C. and Ou, J. (2023), "Fatigue life evaluation of parallel steel-wire cables under the combined actions of corrosion and traffic load", *Structural Control and Health Monitoring*, Vol. 2023, p. 5806751.

Yuan, Z., Sun, G., Wu, X., Li, H. and Kong, L. (2022), "Research on vertical deformation and predeformation control of three-tower connected super high-rise structure during construction", *The Structural Design of Tall and Special Buildings*, Vol. 31 No. 4, p. e1913.

Yuan, Z., Sun, G., Wu, X., Li, H. and Kong, L. (2023), "Equivalent conversion investigation of environmental corrosion of suspenders in long-span suspension bridge", *Anti-Corrosion Methods and Materials*, Vol. 70 No. 6, pp. 533-541.

Yuan, Z., Wang, H., Li, R., Wang, L., Mao, J. and Zong, H. (2024a), "Corrosion fatigue analysis of suspenders on continuous suspension bridge under combined action of wind and traffic", *Engineering Failure Analysis*, Vol. 167, p. 109037.

Yuan, Z., Wang, H., Li, R., Mao, J. and Gao, H. (2024b), "Influence of main cable Displacement-Controlled device of long-span suspension bridge on seismic performance of structure", *International Journal of Structural Stability and Dynamics*, p. 2650067.

Yuan, Z., Wang, H., Li, R., Wang, L., Mao, J. and Zong, H. (2025), "Effect of displacement-controlled suspender on fatigue life of suspension structure under action of wind and traffic", *Structures*, Vol. 73, p. 108513.

Zhang, X., Yu, L., Yin, H. and Lai, K. (2022), "Integrating data augmentation and hybrid feature selection for small sample credit risk assessment with high dimensionality", *Computers & Operations Research*, Vol. 146, p. 105937.

Zhu, X., Xing, C., Wang, H., Zhong, J. and Zhang, Y. (2024), "Probabilistic ductile deformation limit state prediction of monolithic exterior shear keys based on quantile regression machine learning techniques", *Engineering Structures*, Vol. 317, p. 118610.

Corresponding author

Hao Wang can be contacted at: wanghao1980@seu.edu.cn